

JAAS

Accepted Manuscript



This is an *Accepted Manuscript*, which has been through the Royal Society of Chemistry peer review process and has been accepted for publication.

Accepted Manuscripts are published online shortly after acceptance, before technical editing, formatting and proof reading. Using this free service, authors can make their results available to the community, in citable form, before we publish the edited article. We will replace this *Accepted Manuscript* with the edited and formatted *Advance Article* as soon as it is available.

You can find more information about *Accepted Manuscripts* in the [Information for Authors](#).

Please note that technical editing may introduce minor changes to the text and/or graphics, which may alter content. The journal's standard [Terms & Conditions](#) and the [Ethical guidelines](#) still apply. In no event shall the Royal Society of Chemistry be held responsible for any errors or omissions in this *Accepted Manuscript* or any consequences arising from the use of any information it contains.

Calibration methods in glow discharge optical emission spectroscopy: A tutorial review

Zdeněk Weiss

LECO Instrumente Plzeň, spol. s r.o., Plaská 66, 323 20 Plzeň, Czech Republic

Abstract

Calibration methods used in glow discharge optical emission spectrometry are reviewed. They differ in the ways of handling the variable sputtering rate of different materials. Sputtering rate affects the intensities of emission lines of the elements analyzed and must be corrected for. Algorithms implementing these methods are described, including corrections for line interferences, non-linear calibration functions and the calculation of sputter factors from calibration data. Precision and accuracy is discussed for analysis of medium and high concentrations of the elements and for analysis of low concentrations approaching the limits of detection.

Keywords

glow discharge optical emission spectroscopy, calibration, standard model, line interferences, precision, accuracy, matrix effects

1. Introduction

Glow discharge optical emission spectroscopy (GD-OES) [1-6] is a popular method for routine elemental analysis of metals and alloys and depth profiling of various coatings, with a typical depth ranging from nanometers to more than 100 micrometers. The sample to be analyzed acts as cathode in a glow discharge in argon, in a flat-cathode setup called the Grimm-type source [7]. A typical GD-OES spectrometer is either a multichannel polychromator using photomultipliers as detectors, with a number of built-in channels, each for a fixed wavelength (emission line). Or it can be an instrument with CCD¹ detectors, making it possible to select arbitrarily one or more analytical lines for each element to be analyzed, within a continuous wavelength range. With CCD-based instruments, the selection of analytical lines can be optimized for each specific application. Similarly as other spectroscopies, GD-OES is a relative method and depends on calibration based on reference materials with a known composition. Over the years, different calibration methods have been developed for GD-OES. Traditionally, they are divided into two groups: those for 'bulk' analysis, i.e., analysis of samples the composition of which is not changing with depth, and those for depth profiling. The latter were described thoroughly in the literature about GD-OES [1-3], but much less attention has been paid so far to calibration methods for 'bulk' analysis and their links to the methods for depth profiling. The aim of this article is to review all calibration methods used in GD-OES, show how they are related and which of them is suitable for which applications.

2. Calibration methods in GD-OES

¹ CCD = charge-coupled device, a detector consisting of an array of light-sensitive elements integrated together with the supporting circuitry on a monocrystalline silicon chip

The simplest approach is to consider emission intensities to be proportional to the concentrations of the corresponding elements in the sample (the 'normal-' or 'mode-I' calibration):

$$I_{\lambda(E),M} = \alpha_{\lambda(E)} c_{E,M} \quad (1)$$

Here $I_{\lambda(E),M}$ is the intensity of certain emission line $\lambda(E)$ of an element E , $c_{E,M}$ is the concentration of this element in material M and $\alpha_{\lambda(E)}$ is a proportionality factor. It was recognized very early that this approach works satisfactorily only for samples from within a narrow group of very similar materials with virtually the same matrix, e.g. in analysis of impurities in a pure metal such as e.g. copper or nickel. For more general applications, Eqn. (1) needs to be replaced by a more accurate relation [8-10], namely

$$I_{\lambda(E),M} = R_{\lambda(E)} c_{E,M} q_M \quad (2)$$

where q_M is called the *sputter factor*, depending on the material M analyzed. This factor is the same for all emission lines of all elements observed in analysis of the same material. The proportionality constant $R_{\lambda(E)}$, called the *emission yield*, is characteristic for each line $\lambda(E)$ and is supposed not to depend on the material (matrix) analyzed. Eqn. (2) is sometimes called the standard model of GD-OES and is believed to have a simple underlying physical context [11]: if excitation conditions are not affected by the sample composition, which is true in many situations, intensity $I_{\lambda(E),M}$ will be proportional to the number density n_E of the element E in the discharge, which is proportional to the flux of atoms of this element entering the discharge. And this flux is proportional to the product $c_{E,M} Q_M$ where Q_M is the *sputtering rate*, i.e., the rate at which the material M is sputtered (atomized). Q_M can be measured, but no simple relation exists between Q_M and more fundamental quantities. Eqn. (2) thus holds for $q_M = Q_M$. Also, it will hold for $q_M = \gamma \cdot Q_M$ where γ is an arbitrary constant, common for all matrices, as all emission yields can be multiplied by $1/\gamma$ and Eqn. (2) will remain unchanged. The 'absolute' sputtering rate Q_M is important only for quantification of depth in depth profiling [11]. Frequently, the sputter factor q_M is chosen as the sputtering rate relative to the sputtering rate of a common matrix, such as e.g. pure iron, if sputtered at otherwise the same discharge conditions: $q_M = Q_M / Q_{Fe}$. Sputtering rates of some pure elements are listed in Table 1. In Fig. 1a, the sputtering rate of Zn-Fe binary alloys is plotted as function of their composition [21] and a plot is presented in Fig 1b, showing how intensities of a Fe line and a Zn line are affected [21]. As is common in analytical GD-OES, mass units are used throughout this article, i.e., sputtering rates are expressed as mass-per-second and all concentrations are in weight percent.

Eqn. (2) indicates that a crucial condition for accurate analysis by GD-OES will be the ability to correct for variations of the sputtering rate between different materials to be analyzed. Suppose now for simplicity that just one line (one channel) is recorded for each element. Then the symbol E can be used instead of $\lambda(E)$ in equations (1) and (2). One possible way to more universal calibration methods (modes) than the 'normal' mode mentioned above is to select a 'reference' element P and consider the ratios $I_{E,M}/I_{P,M}$ instead of the bare intensities $I_{E,M}$. From Eqn. (2) it follows

$$\frac{I_{E,M}}{I_{P,M}} = \frac{R_E}{R_P} \frac{c_{E,M}}{c_{P,M}} \quad (3)$$

The sputter factor cancels itself, hence, calibration methods based on Eqn. (3) correct for variations in the sputtering rate of the materials analyzed by using a reference element P as internal standard. If the sputtering rate varies significantly, whilst the concentration of the reference element P remains virtually constant, the ratio $I_{E,M}/I_{P,M}$ will be proportional to the concentration $c_{E,M}$, with the proportionality factor

$$\beta_E = \frac{R_E}{R_P} \frac{1}{c_{P,M}}. \text{ It is therefore possible to define another calibration mode in which } \beta_E \text{ will be the}$$

calibration constant and the concentrations $c_{E,M}$ in unknown samples will be calculated based on the ratios

$I_{E,M}/I_{P,M}$ instead of the bare intensities $I_{E,M}$. This mode is called '*the ratio mode*' or '*mode 2*'. A typical example of an application in which this mode can be used is the analysis of zinc with some minor elements. Minor elements affect very significantly the sputtering rate of zinc and if the concentration of zinc in a set of materials to be analyzed is e.g. > 98% and the rest to 100% are minor elements, this calibration mode can be used with a suitable line of zinc as the reference channel P . Relative variations of c_{Zn} within this class of materials will then be negligible compared to the variations of q_M caused by the presence of different minor elements and differences in the structure of the metal (grain size etc.).

A further sophistication is necessary to avoid the assumption that $c_{P,M}$ remains virtually constant. Eqn. (3) can be understood also as the direct proportionality between the ratio of the intensities $I_{E,M}/I_{P,M}$ and the ratio of the concentrations, $c_{E,M}/c_{P,M}$, with a proportionality factor (a new calibration constant) that can be denoted as $1/\gamma_E$, $1/\gamma_E = R_E/R_P$. This calibration mode is called '*the normalized mode*' or '*mode 3*' and is suitable for applications in which both the sputtering rate and the concentration of the matrix element (the reference element P) vary significantly over the range of the materials to be covered by the calibration. This is the case in analysis of alloys, such as e.g. copper alloys or alloyed steels. It is straightforward to establish the calibration constant γ_E by measuring some reference materials and determining the slope of the resulting calibration curve in the coordinates $I_{E,M}/I_{P,M}$ and $c_{E,M}/c_{P,M}$:

$$\frac{c_{E,M}}{c_{P,M}} = \gamma_E \frac{I_{E,M}}{I_{P,M}} \quad (4)$$

However, when analyzing unknown samples, the quantities that can be directly obtained, based on the calibration, are just the $c_{E,M}/c_{P,M}$ ratios and not the concentrations $c_{E,M}$ themselves. The concentration $c_{P,M}$ of the reference element P in an unknown sample can be calculated, based on the assumption that virtually all elements present at significant concentrations have been analyzed, and, consequently, that the sum of their concentrations is 100% (or 1). The following derivation shows how this can be done:

$$\sum_E \frac{c_{E,M}}{c_{P,M}} = \frac{1}{c_{P,M}} \sum_E c_{E,M} = \frac{1}{c_{P,M}} \quad (5)$$

$$\sum_E \frac{c_{E,M}}{c_{P,M}} = \frac{c_{P,M} + \sum_{E \neq P} c_{E,M}}{c_{P,M}} = 1 + \sum_{E \neq P} \frac{c_{E,M}}{c_{P,M}} \quad (6)$$

Combining Eqns. (5) and (6) and substituting from Eqn. (4) we get

$$\frac{1}{c_{P,M}} = 1 + \sum_{E \neq P} \gamma_E \frac{I_{E,M}}{I_{P,M}} \quad (7)$$

On the right side of this equation are only quantities that are known, either from the analysis of the unknown sample (the intensities) or from calibration (the calibration constants γ_E). Hence, $c_{P,M}$ can be calculated from Eqn. (7) and $c_{E,M}$ can subsequently be calculated from Eqn. (4). Calibration modes 2 and 3 work well only if the reference element P is a matrix element: if the concentration $c_{P,M}$ was low, also $I_{P,M}$ would be a small number and because it is in the denominator of the fraction $I_{E,M}/I_{P,M}$, small random fluctuations of the intensity $I_{P,M}$ would be amplified beyond an acceptable level and the results would become useless.

Calibration modes 2 and 3 mentioned above have an advantage that they correct for variations in the sputtering rate, whilst it is not necessary to know the sputtering rates (sputter factors) of the calibration samples, in order to establish calibration curves and calculate calibration constants. The most robust of the three modes mentioned so far is the 'normalized' mode and this mode is also popular in routine analytical work. Its serious drawback is that the calibration depends on a single reference line of the matrix element

and it may not be simple to find a reference line for which Eqn. (2) would hold accurately enough. This is why the best method for analysis of complex alloys is the 'sputter rate-corrected mode', described below. In that mode, the product $c_{E,M}q_M$ is taken as an independent variable in Eqn. (2) and the intensities are considered to be proportional to it, with a proportionality constant R_E to be determined by calibration and called the emission yield. Similarly as with the normalized mode, the composition of unknown samples is calculated in two steps: first, the products $c_{E,M}q_M$ are calculated from based on the intensities measured, using the emission yields resulting from calibration, and then the unknown sputter factor q_M is calculated by normalization to 100%, in a way analogous to the normalized mode as mentioned above. The resulting expression for the sputter factor of an unknown sample is

$$q_M = \sum_E \frac{I_{E,M}}{R_E} \quad (8)$$

Unlike the normalized mode, in sputter rate-corrected calibrations all the elements analyzed are treated equally, there is no 'reference element'. The importance of the sputter rate-corrected mode is also in that, unlike any other mode, it makes it possible to construct self-consistent calibrations, consistent with Eqn. (2), also in the presence of line interferences and for emission lines the intensity of which is a non-linear function of $c_{E,M}q_M$ (see the section 4).

The explicit formula (8) for the sputtering rate (the sputter factor) makes it possible to determine the sputtering rate as a by-product of the analysis of an unknown sample, which is a prerequisite for the quantification of depth profiles. The sputter rate-corrected mode was in fact developed primarily for depth profiling. In depth profile analysis, calibration is performed with 'bulk' calibration samples as described here and the depth profile data of an unknown sample (intensities-versus-time of sputtering) are then treated in the same way as described above, point-by-point, getting thereby the composition and the sputtering rate as functions of the time of sputtering. To convert the time variable into depth, the sputtering rate is then integrated as function of time. In that procedure, the density of the material sputtered at a given depth is needed. The density can be estimated, based on the composition as resulting from the analysis [1-3, 6, 9-11]. The four calibration methods described in this section are summarized in Table 2.

3. Corrections for line interferences and the background

The overview of the calibration methods in the previous section assumed the basic intensity–concentration relationship given by Eqn. (2). In practice, however, this assumption is never fulfilled accurately. One factor that needs to be accounted for are line interferences. Suppose that a line $\lambda(E)$ of element E has an interference with a line $\lambda(F)$ of another element F , i.e., that the wavelengths $\lambda(E)$, $\lambda(F)$ are so close that they both are collected in the spectral window intended for $\lambda(E)$. Then the total intensity measured at that wavelength, according to Eqn. (2), will be:

$$I_{\lambda,M} = R_{\lambda(E)} c_{E,M} q_M + R_{\lambda(F)} c_{F,M} q_M \quad (9)$$

It is assumed for simplicity that there is a complete overlap between the analytical- and the interfering line. To characterize how strong the interference is, it is possible to examine what will be the relation between the concentrations $c_{E,M}$ and $c_{F,M}$ to produce the same intensity $I_{\lambda,M}$ in the spectral window at $\lambda(E)$.

Let such concentrations be denoted as $\hat{c}_{E,M}$, $\hat{c}_{F,M}$:

$$R_{\lambda(E)} \hat{c}_{E,M} q_M = R_{\lambda(F)} \hat{c}_{F,M} q_M \quad (10)$$

and

$$\frac{\hat{c}_{E,M}}{\hat{c}_{F,M}} = \frac{R_{\lambda(F)}}{R_{\lambda(E)}} \quad (11)$$

This is a constant and can be denoted as α_{EF}^λ ,

$$\alpha_{EF}^\lambda = \frac{R_{\lambda(F)}}{R_{\lambda(E)}} \quad (12)$$

α_{EF}^λ is a dimensionless parameter that can be used as a measure of the magnitude of the line interference: it says what would be the concentration of the analyzed element E that would produce the same intensity as the pure element F ($c_{F,M} = 1$) at the spectral window around $\lambda(E)$. It is worth noting that, unlike individual emission yields, α_{EF}^λ does *not* depend on the instrument function of the spectrometer used (sensitivity as function of the wavelength), but may depend on its resolution: Eqn. (12) assumes that all the light coming from the line $\lambda(F)$ is collected by the channel $\lambda(E)$. If there is only a partial overlap, α_{EF}^λ will be smaller than what Eqn. (12) says and if there is no overlap, α_{EF}^λ will be zero and that interference will vanish. If there are two or more lines of element F in the spectral window of the channel $\lambda(E)$, their contributions to the measured signal in the channel $\lambda(E)$ will add and the numerator in the fraction Eqn. (12) will become the sum of their emission yields, each reduced as mentioned above if there is only a partial overlap with the spectral window of the channel $\lambda(E)$. As an example, in Table 3 the α_{EF}^λ values are listed for line interferences affecting some lines that can be used for determination of hafnium and tantalum in nickel alloys on the LECO GDS500A spectrometer [12], an instrument with a medium spectral resolution of ~ 70 pm. Such a table helps when selecting analytical lines for specific applications: for example, for determination of tantalum in alloys with tungsten, a good candidate will be the line Ta I, 457.431 nm, as it has the weakest interference with tungsten of all the Ta lines considered.

Actually measured intensities usually contain also a non-zero background component, b_E , virtually independent of the sample composition. Following the convention mentioned above that only the subscript E is used instead of $\lambda(E)$, and denoting as $s_{E,F}$ the emission yield of interfering line(s) of another element F at the wavelength $\lambda(E)$, reduced appropriately if not all light from the line $\lambda(F)$ is collected, Eqn. (2) becomes

$$I_{E,M} = R_E c_{E,M} q_M + \sum_{F \neq E} s_{E,F} c_{F,M} q_M + b_E \quad (13)$$

The sum on the right side describes situations in which there are line interferences in the channel $\lambda(E)$ from more elements than just one. Line interferences and the background can now be included in the sputter rate-corrected calibration mode so that the constants R_E , b_E and $s_{E,F}$ in Eqn. (13) are all taken as calibration parameters and can be determined, element by element (channel by channel) by linear least squares fitting of the calibration data [13], by minimizing the weighted sum of squared residuals, χ^2 :

$$\chi_E^2 = \sum_M \omega_{E,M} \left(I_{E,M} - R_E c_{E,M} q_M - \sum_{F \neq E} s_{E,F} c_{F,M} q_M - b_E \right)^2 \quad (14)$$

where $\omega_{E,M}$ is the statistical weight. It is necessary to make sure that a sufficient number of calibration points exists for each element, so that the system of equations (13) in which E is the same but the M -s are different remains overdetermined. If there are n calibration points (i.e., certified concentration of the element E is available for n calibration samples and the intensities for them have been collected), there will be $n - k - 2$ degrees of freedom where k is the number of inter-element corrections. An example of a linear sputter rate- and line interference-corrected calibration function with a significant background signal and significant inter-element corrections is in the plot in Fig. 2. It is the Mo I line at 418.832 nm, in a calibration covering a wide range of nickel alloys on an instrument with a medium resolution of ~ 70 pm. Calibration parameters were calculated with 14 degrees of freedom, for $n = 22$ and $k = 6$, with corrections for line interferences from Fe, Ti, Nb, V, W, Ta. This is just one of several molybdenum lines that can be used for analysis of Mo in nickel alloys. The format of the plot follows the convention common in GD-OES: The 'raw' data, i.e. the points representing intensity-versus-concentration, are printed in magenta, with the abscissa being the intensity coordinate. The 'corrected' data, i.e. $(I_{E,M} - \sum I_{F,M})$ versus $(c_{E,M} \cdot q_M)$ are

printed in red and every point of the 'raw' data is connected with the corresponding 'corrected' point by a line in turquoise. In this convention, an inter-element correction shifts the calibration point to the left and the correction for the sputtering rate shifts the point up or down, depending on whether $q_M > 1$ or $q_M < 1$. The emission yield R_E is the reciprocal of the slope of the calibration curve. The points on the x-axis represent materials with virtually no molybdenum, hence, the intensities observed for those materials originate from line interferences and the background and the corresponding 'corrected' (red) points have the x-coordinate close to the background intensity, b_{Mo} .

When analyzing unknown samples, the question arises how to apply the calibration to the measured intensities in order to obtain the resulting sample composition. For an arbitrary sample, Eqn. (13) can be understood as a linear transform between the vector of the measured intensities, $\mathbf{I} = (I_1, I_2, \dots, I_E)^T$ and the vector of concentrations of the corresponding elements in the sample, $\mathbf{c} = (c_1, c_2, \dots, c_E)^T$. The superscript T means that both vectors are considered as column vectors. Eqn. (13), representing this transform, can be rewritten as

$$\mathbf{I} = \mathbf{R} \mathbf{x} + \mathbf{b} \quad (15)$$

where $\mathbf{x} = q \mathbf{c}$ is the vector of sputter rate-corrected concentrations, \mathbf{b} is the vector of the background intensities, $\mathbf{b} = (b_1, b_2, \dots, b_E)^T$, and \mathbf{R} is the matrix of emission yields of the 'analytical' and the 'interfering' lines, the former being on the diagonal:

$$\mathbf{R} = \begin{bmatrix} R_1 & s_{1,2} & \dots & s_{1,E} \\ s_{2,1} & R_2 & & s_{2,E} \\ \cdot & & & \cdot \\ s_{E,1} & \dots & s_{E,E-1} & R_E \end{bmatrix} \quad (16)$$

The solution of Eqn. (15) is

$$\mathbf{x} = \mathbf{R}^{-1}(\mathbf{I} - \mathbf{b}) \quad (17)$$

where \mathbf{R}^{-1} is an inverse to the matrix \mathbf{R} . If there are no interferences, individual equations for different elements are independent (not coupled together) and the matrix \mathbf{R} is diagonal, with zeros in all cells outside the diagonal. It can be denoted as \mathbf{R}_0 . This corresponds to Eqn. (13) without the second term on the right side. For such situation, the solution is trivial:

$$\mathbf{R}_0^{-1} = \begin{bmatrix} R_1 & 0 & \dots & 0 \\ 0 & R_2 & & \cdot \\ \cdot & & & 0 \\ 0 & \dots & 0 & R_E \end{bmatrix}^{-1} = \begin{bmatrix} 1/R_1 & 0 & \dots & 0 \\ 0 & 1/R_2 & & \cdot \\ \cdot & & & 0 \\ 0 & \dots & 0 & 1/R_E \end{bmatrix}$$

In the presence of line interferences, Eqn. (15) can be solved by suitable methods of linear algebra. The following iterative process was found to work well:

$$\mathbf{x}^0 = \mathbf{R}_0^{-1}(\mathbf{I} - \mathbf{b}), \quad (18)$$

$$\mathbf{x}^{n+1} = \mathbf{R}_0^{-1}[\mathbf{I} - \mathbf{b} - (\mathbf{R} - \mathbf{R}_0) \mathbf{x}^n] \quad (19)$$

whilst in each step, if any component of the vector \mathbf{x}^{n+1} comes up as a negative value, it is set to zero before calculating the next iteration. The superscripts denote individual approximations. Typically less than 5 iterations were needed when calculating results of analysis of nickel alloys from the example to which Table 3 refers. A fast convergence of this process occurs because the non-diagonal elements s_{ij} in

the matrices defined by Eqn. (16) are typically much smaller than the diagonal elements R_i (i.e., the interfering lines of other elements are much weaker than the analytical line of the element affected).

Eqns. (18) and (19), if written in a non-matrix notation, would become

$$x_E^0 = \frac{1}{R_E} (I_{E,M} - b_E) \quad (20)$$

$$x_E^{n+1} = \frac{1}{R_E} \left(I_{E,M} - b_E - \sum_{F \neq E} S_{E,F} x_F^n \right) \quad (21)$$

where $x_E = c_{E,M} q_M$. It should be noted that these calculations can be done with any number of lines (channels) for an element and if more than one line is used, the resulting x_E or the concentration c_E can be calculated as the average or the median over all the lines of the element E that are measured. The sputter factor q , necessary to convert x_E into the concentration c_E , is determined by normalization, as described in the previous section.

In calibration mode 3, it would not be practical to use $c_{F,M} q_M$ as an independent variable for the correction of line interferences. The standard model of GD-OES is supposed to have an universal validity and virtually all lines in the spectrum, including the interfering lines, should follow Eqn. (2). Hence, instead of $c_{F,M} q_M$, intensity of another line of element F can be used to correct for the line interference and the correction related to element F will be proportional to the intensity of that line. A logical choice is to use for that purpose the analytical line for element F (suppose now again for simplicity that only one analytical line is measured for each element). The corresponding proportionality constant let be denoted as σ_{EF} . In the presence of line interferences, Eqn. (4) becomes

$$\frac{c_{E,M}}{c_{P,M}} = \gamma_E \frac{I_{E,M} + \sum_F \sigma_{EF} I_{F,M}}{I_{P,M}} = \gamma_E \frac{I_{E,M}}{I_{P,M}} + \sum_{E \neq F} \kappa_{EF} \frac{I_{F,M}}{I_{P,M}} \quad (22)$$

where $\kappa_{EF} = \gamma_E \sigma_{EF}$. Unlike the factors α_{EF}^λ from the sputter rate-corrected mode, Eqn. (12), these correction factors, κ_{EF} , have no wider use to characterize the corresponding interference, as they depend on the selection of the lines $\lambda(F)$, $\lambda(P)$. Note that, here, $\lambda(F)$ is *not* the interfering line itself, but another line of element F to which the intensity of the interfering line is supposed to be proportional. The background term, if added to the numerator on the right side of Eqn. (4), would be divided by the intensity of the matrix element that may vary between different materials to be analyzed. Therefore, mode 3 should be used rather for medium- and higher concentrations, certainly higher than the the background-equivalent concentration, $(BEC)_E = b_E/R_E$ for a sample with $q_M = 1$. From Eqn. (22), it is apparent that, with this stipulation, the correction for interferences can be made fully within mode 3, i.e., with the intensity ratios as the basic quantities. Again, γ_E and κ_{EF} are to be considered as calibration constants. An interesting situation will arise if the line $\lambda(F)$ that is used to correct for an interference caused by element F is itself disturbed by line interference(s) from another element(s). Then the line intensity I_E can be expressed as a linear combination not only of the intensities of the lines $\lambda(E)$ and $\lambda(F)$, but also of analytical lines of the elements the lines of which interfere with $\lambda(F)$. If these additional corrections are included, those line interferences in the channel $\lambda(F)$ will be correctly accounted for. Concerning the analysis of unknown samples, it is straightforward to calculate the c_E/c_P ratios from Eqn. (22), as all the quantities on its right side are either measured or known from the calibration. c_P can then be calculated by normalization, as it was described in the previous section.

It may seem attractive to replace by intensities $I_{E,M}$ the $c_{F,M} q_M$ products in their role as independent variables for inter-element corrections also in the sputter rate-corrected mode, similarly as it was done in mode 3. But a better approach is to work with corrections based on $c_{F,M} q_M$ rather than the intensities. This makes it possible to use an 'intelligent' procedure for determining accurately $c_{F,M} q_M$, e.g. by using several

lines for the element F instead of relying on a single line and hoping that it follows accurately the standard model, Eqn. (2). To incorporate corrections for line interferences in modes 1 and 2 would be an easy exercise based on the concepts presented above and is not shown here.

4. Non-linear calibration functions

Intensities of some lines are not proportional to (cq) but grow with the increase of (cq) more slowly than linearly. This behavior is due to self-absorption of resonance radiation in the source and occurs, besides resonance lines, also for lines associated with transitions to some highly populated metastable levels. Theoretical functions describing the experimental intensity-versus- (cq) curves can be calculated, based on the *curve-of-growth* (COG) theory [14- 17], that relates emission intensities to the optical density. In analytical applications, empirical functions are used, established by calibration, and represented by a higher-order polynomial instead of the direct proportionality expressed by Eqn. (2). In a quadratic approximation, sufficient for a majority of analytically important lines with a non-linear intensity response, Eqn. (2) can be replaced by

$$I_{\lambda(E),M} + a_E I_{\lambda(E),M}^2 = R_{\lambda(E)} c_{E,M} q_M \quad (23)$$

In the sputter rate-corrected calibration mode, the parameter a_E from Eqn. (23) becomes a new calibration constant and the complete calibration function for element E with a non-linear intensity response will be expressed by the following equation:

$$I_{E,M} + a_E I_{E,M}^2 = R_E c_{E,M} q_M + \sum_{F \neq E} s_{E,F} c_{F,M} q_M + b_E \quad (24)$$

It is not very common in analytical chemistry to describe calibration relations in the form of implicit functions like those defined by Eqn. (23) or (24), but here it is the best way. The modified χ^2 function to be minimized by linear least squares fitting² to calculate the calibration constants will be

$$\chi_E^2 = \sum_M \omega_{E,M} \left(a_E I_{E,M}^2 + I_{E,M} - R_E c_{E,M} q_M - \sum_{F \neq E} s_{E,F} c_{F,M} q_M - b_E \right)^2 \quad (25)$$

Compared to the linear calibration function, there will be one less degree of freedom, namely $n - k - 3$, where n is the number of calibration points for element (channel) E and k is the number of inter-element corrections affecting this element (channel). To calculate $\mathbf{x} = q \mathbf{c}$ for a sample measured as an unknown, with already established calibration constants, the iterative process mentioned in the previous section will become

$$x_E^0 = \frac{1}{R_E} (a_E I_{E,M}^2 + I_{E,M} - b_E) \quad (26)$$

$$x_E^{n+1} = \frac{1}{R_E} \left(a_E I_{E,M}^2 + I_{E,M} - b_E - \sum_{F \neq E} s_{E,F} x_F^n \right) \quad (27)$$

If the quadratic approximation is not sufficient, higher terms could be added similarly as the quadratic term. The corresponding modifications of Eqns. (24)-(27) are obvious.

As far as mode 3 is concerned, suppose that Eqn. (23) is used instead of Eqn. (2) for a line of an element E having a non-linear intensity response. If Eqn. (23) is divided by the intensity $I_{P,M}$ of a reference line of the matrix element P that obeys Eqn. (2), the following will be obtained:

² it is still *linear* regression, as the calibration function (24) is linear in all the parameters to be determined: a_E , R_E , s_{EF} and b_E

$$\frac{I_{E,M}}{I_{P,M}} + a_E \left(\frac{I_{E,M}}{I_{P,M}} \right)^2 R_P c_{P,M} q_M = \frac{R_E c_{E,M}}{R_P c_{P,M}} \quad (28)$$

This equation is still in conformity with the mode 3 ($I_{E,M}/I_{P,M}$ versus $c_{E,M}/c_{P,M}$), except that the coefficient by the quadratic term on the left side contains the product $c_{P,M}q_M$, which is *not* constant but varies between different materials to be analyzed. Its variations would impair accuracy of such calibration and make it worse than what can be achieved with the sputter rate-corrected mode. However, despite the variations, this term still represents a small, non-zero correction of an approximately correct magnitude and the fit will be therefore slightly better than if the quadratic term is omitted, i.e., with a linear calibration function.

5. Sputter factors of calibration samples

As follows from the previous sections, the sputter rate-corrected mode is the best calibration method for analysis of complex alloys in a wide range of concentrations. Its disadvantage is that reference materials with known sputtering rates (sputter factors) are needed for calibration. Sputtering rate of a material can be determined directly: the sample is sputtered in the Grimm-type source for certain time, the volume of the resulting erosion crater is measured by scanning profilometry [18, 19] and the sputtering rate can then be calculated as the mass sputtered per time unit. An example of such measurement is described by Fig. 3. It should be noted that direct measurements of the sputter rate may be affected by roughness development of the sputtered surface and uneven crater profiles [29, 30] and the precision achieved may become a limiting factor. Relative sputtering rates of pure elements in Table 1 should be considered as approximate. Also, it should be stressed that, when comparing sputtering rates of different materials, it is important to specify what is understood as 'the same discharge conditions' (e.g. constant voltage - constant current).

Another option is to determine sputter factors of some (or all) calibration samples from the calibration itself. The information for doing so is inherently included in the calibration data. Suppose first that the sputter factors are known for p of the n reference samples included in the calibration and regard the remaining q_M -s in Eqn. (13) as additional unknown variables. This means that all the equations for different E -s and M -s are taken together as the set to be solved. If the number of the elements (channels) is m and if, for simplicity, all the elements are certified in all the reference samples, there will be nm equations for $2m + k + (n - p)$ unknowns, where k is the total number of inter-element corrections. The χ^2 function to be minimized to solve this system by least squares fitting will be

$$\chi^2 = \sum_E \chi_E^2 = \sum_E \sum_M \omega_{E,M} \left(I_{E,M} - R_E c_{E,M} q_M - \sum_{F \neq E} s_{E,F} c_{F,M} q_M - b_E \right)^2 \quad (29)$$

The problem is that the resulting system of normal equations is non-linear in the unknown variables R_E and q_M : it contains products ($R_E q_M$) in which both R_E and q_M are unknown. Possible ways of solving this system are described in [20]. In practice, the most common method is to calculate first the R_E , b_E and $s_{E,F}$ parameters for some channels, based on a sub-set of all calibration samples for which the sputter factors are known, and then take the thereby established calibration functions as the basis for calculating the q_M -s of the remaining calibration samples. The corresponding system of equations will then be linear because the R_E -s in the ($R_E q_M$) products in which the q_M -s are unknown will be constants, determined in the preceding step. An example of this procedure is shown in Fig. 4. The data come from the calibration mentioned above, from which also the examples in Figs. 2, 3 and Table 3 originate. Calibration functions of two measured lines, Co I, 240.725 nm (Fig. 4, top) and Cr II, 283.563 nm (Fig. 4, bottom), were used to calculate the sputter factor of a sample called IMZ-185. The pair of the points corresponding to this sample is connected by a blue line instead of turquoise³. The calibration functions (grey lines) are well defined, by a number of other calibration samples with known sputter factors (red points). In each plot,

³ IMZ-185 is a certified reference material, a nickel alloy, made by the Institut Metalurgii Żelaza, Gliwice, Poland

there is a dashed red line representing the set of all possible 'corrected' points belonging to the sample IMZ-185, for different sputter factors varying between $q_M = 1$ and $q_M = 3$. Parametric equation of this line is

$$I_E - I_{E,IMZ185} = - \sum_{F \neq E} s_{E,F} c_{F,IMZ185} q \quad (E = Co, Cr) \quad , \quad (30)$$

in the coordinates cq, I_E , with q as the parameter and all the other quantities constant (calibration constants $s_{E,F}$ and the constants $I_{E,IMZ185}$, $c_{F,IMZ185}$ that are specific for this particular sample). The intersection of this line with the calibration curve is the point corresponding to the correct sputter factor of the sample IMZ-185. In conformity with the standard model (Eqns. (2), (13)), both the chromium and cobalt calibrations give the same sputter factor, $q_{IMZ185} = 1.87 \pm 0.02$.

6. Precision and accuracy

To assess the uncertainty associated with the experiments and its propagation in the subsequent calculations is important for two reasons: (1) to estimate the level of uncertainty in the analysis of unknown samples and (2) to check how well a particular calibration reflects the actual signal response. If there are significant deviations between the predicted and the observed response for some calibration samples, the first step is to make sure that the calibration model was used correctly, i.e., that the right inter-element corrections have been applied, correct sputter factors have been used, etc. And only if significant deviations still persist, the standard model itself should be considered questionable for that particular situation, i.e., the deviations should be treated as matrix effects. The magnitude of the matrix effects for an element E can be expressed by the standard error $(SE)_E$, defined as [22]

$$(SE)_E = \sqrt{\frac{1}{f} \sum_M (c_{E,M}^{certified} - c_{E,M}^{predicted})^2} \quad (31)$$

where the summation runs over all calibration samples with a certified concentration of element E and f are degrees of freedom, i.e. the number of the calibration samples defining the calibration curve for element E minus the number of calibration parameters corresponding to that curve. Standard error is a general measure of matrix effects in any analytical method. An alternative that is better for GD-OES, the median error, is mentioned below. See Eqn. (33) and the comments thereby.

Propagation of uncertainty in the GD-OES analysis was described in [23]. It is based on general rules of error analysis [24]. If a line $\lambda(E)$ behaves according to the standard model, the most significant component of the resulting uncertainty are random fluctuations of the measured intensities, $\delta I_{E,M}$. For medium and high concentrations of the elements analyzed for which the errors introduced by fluctuations of the background and by line interferences can be neglected, the following result applies for the sputter rate-corrected calibration mode: If the uncertainties $\delta I_{E,M}$ are random and independent, the error $\delta c_{E,M}$ of the analysed concentration will be [23]

$$\left(\frac{\delta c_{E,M}}{c_{E,M}} \right)^2 = (1 - c_{E,M})^2 \left[\left(\frac{\delta I_{E,M}}{I_{E,M}} \right)^2 + \left(\frac{\delta R_E}{R_E} \right)^2 \right] + \sum_{F \neq E} c_{F,M}^2 \left[\left(\frac{\delta I_{F,M}}{I_{F,M}} \right)^2 + \left(\frac{\delta R_F}{R_F} \right)^2 \right] \quad (32)$$

where δR_E , δR_F are prospective errors of emission yields. In multiple analyses of a single sample, only the intensities are changing, hence, the first term in each square bracket represents the random error and the second term the systematic error due to the (maybe biased) emission yields used for the calculations, i.e. the systematic error within the standard model. From Eqn. (32), the following conclusions can be inferred (the second follows from the first):

1. Because of normalization, an error in analysis of any element will affect all the other elements. Contributions to the *relative* error of $c_{E,M}$ caused by errors in intensities and emission yields of the other elements are proportional to their concentrations.
2. At high concentrations of the element E (close to 1), the contributions to $\delta c_{E,M}/c_{E,M}$ from $\delta I_{E,M}$ and δR_E are suppressed by normalization and the contributions from the other elements are small, because their concentrations are small. A trivial consequence of this is that, if analyzing pure element E with some minor elements, relative error of its concentration $c_{E,M}$ will always be small.

The assumption of the errors $\delta I_{E,M}$ $\delta I_{F,M}$ being random and independent is crucial: frequently, a substantial part of the intensity variations comes from a variable sputtering rate of the matrix at different spots on the same sample. In such case, the variations $\delta I_{E,M}$, $\delta I_{F,M}$ are highly correlated, a substantial cancellation of the errors occurs and Eqn. (32) significantly overestimates the actual error. The formula (32) is useful for practical applications. However, for testing the validity of the standard model, Eqn. (32) is not very good because the normalization would mix up prospective deviations associated with different elements and impair thus our ability to identify the matrix effects. Therefore, such tests are usually made so that the calibration is checked for self-consistency, element by element. This can be done so that the differences $(q_M c_{E,M})^{\text{certified}} - (q_M c_{E,M})^{\text{predicted}}$ are compared with the uncertainties expected within the standard model. If they are significantly higher for some samples, they indicate the existence of matrix effects. In this context, it is worth to mention another measure of the overall accuracy than the standard error, Eqn. (31): standard error describes well situations in which big deviations between the predicted and the actual quantities are very rare, e.g., are normally distributed. But for calibrations in GD-OES it may not necessarily be the case and then a better measure is the *median error*, that for the $(q_M c_{E,M})$ products is defined as

$$ME(cq)_E = \text{median}_M \left(\left| (q_M c_{E,M}^{\text{certified}}) - (q_M c_{E,M})^{\text{predicted}} \right| \right) \quad (33)$$

An example of a matrix effect in the analysis of nickel alloys mentioned above is in Fig. 5. The plot on top shows the calibration curve of the Ni I line at 301.200 nm, which is free of matrix effects: with relevant corrections for line interferences and quadratic calibration function, it gives a very good fit between the measured and the predicted $q_M c_{E,M}$ values. On the other hand, e.g. the Ni II line at 216.910 nm clearly exhibits a matrix effect – see its calibration function in the bottom plot. Both calibrations use identical samples with the same sputter factors. A very similar pattern as for the latter line was observed for a number of other Ni II lines with excitation energies between 6.4 and 7.0 eV. It is likely that this matrix effect is related to glow discharge excitation of nickel. Although some attempts have been made to explain various excitation-related matrix effects in GD-OES, no systematic treatment of this topic exists. This example illustrates how critical it is to choose the 'right' lines for analytical purposes. In particular, this concerns the reference lines $\lambda(P)$ for the 'ratioed' and the 'normalized' calibration modes. If the line Ni II, 216.910 nm was used as $\lambda(P)$, it would deteriorate this calibration beyond a tolerable level.

With a reasonably good instrument and typical certified reference materials, it is usually impossible to achieve full self-consistency within the standard model, i.e. the situation that all observed deviations at medium and high concentrations can be attributed to random uncertainties of the measurements. A typical accuracy of the standard model for metals and alloys in GD-OES at medium and high concentrations is about 1-2% relative and the deviations are comparable with the estimated uncertainty of the certified concentrations of the reference materials used [23]. At low concentrations of the analyzed element E , it can be shown [23] that the precision is the worse the higher is the $(BEC)_E$ and if some elements causing line interferences at $\lambda(E)$ are present, then the precision is the worse the higher are their concentrations $c_{E,M}$ and the corresponding α_{EF} coefficients defined by Eqn. (12):

$$(\delta c_{E,M})^2 = \frac{(BEC)_E^2}{q_M^2} \left[\left(\frac{\delta I_{E,M}}{b_E} \right)^2 + \left(\frac{\delta b_E}{b_E} \right)^2 \right] + \sum_F c_{F,M}^2 \alpha_{EF}^2 \left[\left(\frac{\delta c_{F,M}}{c_{F,M}} \right)^2 + R_E^2 \left(\frac{\delta \alpha_{EF}}{\alpha_{EF}} \right)^2 \right] \quad (34)$$

On the right side of Eqn. (34), the ratio $\delta I_{E,M}/b_E$ represents a random component of the uncertainty (the variability of replicate measurements of the intensity $I_{E,M}$, relative to the background b_E) and the ratios $\delta b_{E,M}/b_E$ and $\delta \alpha_{EF}/\alpha_{EF}$ represent systematic components (prospective errors in the constants b_E , α_{EF} that may have arisen in the calibration). The ratios $\delta c_{F,M}/c_{F,M}$ are supposed to be small (they are the second-order components of the combined uncertainty $\delta c_{E,M}$) and also the ratio $\delta R_E/R_E$, neglected in Eqn. (34), is supposed to be much smaller than $\delta \alpha_{EF}/\alpha_{EF}$. The latter assumption means that the line interference from element F is supposed to be 'weak', i.e., that the analytical line $\lambda(E)$ is much stronger than the disturbing line $\lambda(F)$. With this simplification, the final expression for the uncertainty $\delta c_{E,M}$ in the approximation of a low concentration $\delta c_{E,M}$ is

$$(\delta c_{E,M})^2 = \frac{(BEC)_E^2}{q_M^2} \left[\left(\frac{\delta I_{E,M}}{b_E} \right)^2 + \left(\frac{\delta b_E}{b_E} \right)^2 \right] + \sum_F c_{F,M}^2 R_E^2 (\delta \alpha_{EF})^2 \quad (35)$$

The random component of the uncertainty in Eqn. (35), i.e. the variations of the observed intensity, $\delta I_{E,M}$, depend on the concentration(s) of the interfering element(s) and frequently limit the overall performance of the method for low concentrations of the analytes. The designation $\delta I_{E,M}$ should be understood in this context as the total intensity measured in the spectral window around $\lambda(E)$. It should be noted that all these considerations presume the validity of the standard model, Eqn. (2). In the presence of matrix effects, additional systematic errors may occur. Accuracy and precision in the GD-OES analysis can be considerably improved by a parallel use of several lines for a single element, because of partial cancellation by averaging of random errors and weak matrix effects.

7. Conclusions and final remarks

A systematic description of calibration methods used in GD-OES was presented and common ways of calculating calibration parameters and the concentrations of the elements analyzed in unknown samples were reviewed. For each calibration method, it was explained which assumptions and conditions must be fulfilled to achieve an acceptable analytical performance. The concepts described in the previous sections were illustrated on an example of the analysis of a wide range of nickel alloys on the LECO GDS500A spectrometer. Calibration methods described here are relevant to the analysis of conductive materials, which is the main application domain of GD-OES. Besides that, attempts have been made to develop also calibration strategies aimed at depth profiling of non-conductive layers by GD-OES [31]. Discussion about various approaches used for that purpose is beyond the scope of this article.

In every analytical technique, there is a strong link between instrumental developments and the progress in analytical capabilities. In GD-OES, it was the introduction of the dynamic-, feedback-based control of the glow discharge by mass-flow controllers 20 years ago, combined with a remarkable progress in electronics and computer technology, that led to an advent of quantitative depth profiling. Another big step forward was the introduction of commercial spectrometers with CCD detectors ca 10 years ago. They opened access to the 'complete' spectra, in contrast to a limited number of carefully selected lines, mostly one line per element, in classical polychromators with photomultiplier detectors. This new dimension of the GD-OES analysis has been reflected by on-going attempts to explore the use of different lines for analytical purposes. At present, this exploratory stage is still in progress and empirical evidence is mounting, concerning the properties of different emission lines of analytically important elements. A remarkable accuracy of the standard model for many lines and a clear existence of matrix effects in other lines sets a goal to explain these matrix effects and develop more advanced calibration models, based on a better

understanding of the fundamental processes involved. This should ultimately lead to an overall improvement of accuracy of GD-OES as a method.

References

1. R.K. Marcus and J.A.C. Broekaert (Eds.), *Glow Discharge Plasmas in Analytical Spectroscopy*, J. Wiley, New York, 2003
2. R. Payling, D. Jones and A. Bengtson (Eds.), *Glow Discharge Optical Emission Spectrometry*, J. Wiley, New York, 1997
3. T. Nelis, R. Payling, *Glow Discharge Optical Emission Spectroscopy: A Practical Guide*, RSC Analytical Spectroscopy Monographs, The Royal Society for Chemistry, Cambridge, 2003
4. N. Jakubowski, R. Dorka, E. Steers and A. Tempez, Trends in glow discharge spectroscopy, *J. Anal. At. Spectrom.*, 2007, **22**, 722-735
5. Ph. Belenguer, M. Ganciu, Ph. Guillot, Th. Nelis, Pulsed glow discharges for analytical applications, *Spectrochim. Acta, Part B*, 2009, **64**, 623-641
6. V. Hoffmann and A. Quentmeier, Glow Discharge Optical Emission Spectroscopy (GD-OES), in *Surface and Thin Film Analysis: A Compendium of Principles, Instrumentation and Applications*, Second Edition (eds G. Friedbacher and H. Bubert), Wiley-VCH Verlag GmbH & Co. KGaA, Weinheim, 2011
7. W. Grimm, Eine neue Glimmentladungslampe für die optische Emissionsspektalanalyse, *Spectrochim. Acta, Part B*, 1968, **23**, 443-454
8. P.W.J.M. Boumans, Studies of sputtering in a glow discharge for spectrochemical analysis, *Anal. Chem.*, 1972, **44**, 1219-1228
9. J. Takadoum, J.C. Pirrin, J. Pons-Corbeau, R. Berneron and J.C. Charbonnier, Comparative study of ion implantation profiles in metals, *Surf. Interface Anal.*, 1984, **6**, 174 – 183
10. K. Suzuki, K. Nishizaka and T. Ohtsubo, Correction method for matrix effect (quantitative analysis of alloy plating layers using GDS-I), *Transactions ISIJ*, 1984, **24**, B-259
11. Z. Weiss, Emission yields and the standard model in glow discharge optical emission spectroscopy: Links to the underlying physics and analytical interpretation of the experimental data, *Spectrochim. Acta, Part B*, 2006, **61**, 121 – 133
12. K.A. Marshall, P.M. Willis, Centered sphere spectrometer, US Patent 6023330, 1998
13. J. Kragten, Least-squares polynomial curve-fitting for calibration purposes, *Anal. Chim. Acta*, 1990, **241**, 1-13
14. A.C.G. Mitchell and M.W. Zemansky, *Resonance Radiation and Excited Atoms*, Cambridge University Press, 1934
15. I.B. Gornushkin, J.M. Anzano, L.A. King, B.W. Smith, N. Omenetto and J.D. Winefordner, Curve of growth methodology applied to laser-induced plasma emission spectroscopy, *Spectrochim. Acta, Part B*, 1999, **54**, 491-503
16. C.D. West and H.G.C. Human, Self-absorption and Doppler temperatures of emission lines excited in a glow discharge lamp, *Spectrochim. Acta, Part B*, 1976, **31**, 81-92
17. A. Thorne, U. Litzén and S. Johansson, *Spectrophysics : principles and applications*, Springer, Berlin, 1999

18. R. Chmelík and Z. Harna, Surface profilometry by a parallel-mode confocal microscope, *Opt. Eng.*, 2002, **41**, 744-745
19. L. Wilken, V. Hoffmann, K. Wetzig, Erosion rate measurements for GD-OES, *J. Anal. At. Spectrom.*, 2003, **18**, 1141-1145
20. Z. Weiss, New method of calibration for glow discharge optical emission spectrometry, *J. Anal. At. Spectrom.*, 1994, **9**, 351-354
21. S. Suzuki and K.-I. Suzuki, Zinc-Iron Coatings, Chapter 12.2 in Ref [2], pp. 575-581
22. ASTM standard E 1009 – 95 (2006): *Standard Practice for Evaluating an Optical Emission Vacuum Spectrometer to Analyze Carbon and Low-Alloy Steel*
23. Z. Weiss, Propagation of uncertainty in multi-matrix analysis by GD-OES, *J. Anal. At. Spectrom.*, 2001, **16**, 1275-1282
24. J.R.Taylor, *An Introduction to Error Analysis*, 2nd edition, University Science Books, Sausalito, California, 1997
25. A. Bengtson, L. Danielsson, Depth profiling of thin films using a Grimm-type glow discharge lamp, *Thin Solid Films*, 1985, **124**, 231-236
26. P.W.J.M. Boumans, Studies of Sputtering in a Glow Discharge for Spectrochemical Analysis, *Anal. Chem.*, 1972, **44**, 1219-1227
27. J.B. Ko, New designs of glow discharge lamps for the analysis of metals by atomic emission spectroscopy, *Spectrochim. Acta, Part B*, 1984, **39**, 1405-1423
28. A. Raith, Glow Discharge Mass Spectrometry, in Ref. [2], Chapter 15.4., p.753
29. M. Dogan, K. Laqua and H. Massman, Spektrochemische Analysen mit einer Glimmentladungslampe als Lichtquelle—I: Elektrische Eigenschaften, Probenabbau und spektraler Charakter *Spectrochim. Acta, Part B*, **26**, 1971, 631-649.
30. Z. Weiss, Analysis of graphitized cast irons by optical emission spectroscopy: matrix effects in the glow discharge and the spark excitation, *Spectrochim. Acta, Part B*, **51**, 1996, 863-876
31. A. Bengtson, T. Nelis, The concept of constant emission yield in GDOES, *Anal. Bioanal. Chem.* **385**, 2006, 568-585

Table 1Compilation of sputtering rates of some pure elements relative to iron¹

Element	Q_M/Q_{Fe}					
	Ref. [3]	(this work)	Ref. [25]	Ref. [26]	Ref. [27]	Ref. [28]
Al	0.37, (0.34-0.39)	0.405	0.396	0.382	0.36	
Ag	9.3	8.5				7.7
Au	8.1, (5.0-11)	12.6			14.7	
Co	1.8, (1.2-2.4)	1.26				
Cr	1.0, (0.77-1.1)	0.88	0.76			
Cu	3.5, (3.4-3.6)	3.57	3.24	3.8	3.1	3.41
Mo	1.3, (1.2-1.4)	1.4		1.78		
Nb	0.71	0.72				
Ni	1.5, (1.49-1.52)	1.55	1.8	1.64	1.3	1.59
Pb	17					10.3
Si	0.21, (0.17-0.25)					
Sn	6.5	5.3	5.2			
Ta	3.4	2.6		3.7		
Ti	0.43, (0.427-0.430)	0.44				
V	0.50	0.30				
W	2.9, (2.5-3.3)	3.0		3.6	3.4	
Zn	8.2, (7.8-8.6)	6.9	7.1	7.5	7.3	3.8
Zr	0.77, (0.50-1.0)	1.07				

¹ The data in this table concern sputtering rates in the Grimm-type glow discharge and are different from the rates observed in sputtering by ion beams in high-vacuum or ultra-high-vacuum conditions

Table 2

Calibration methods in GD-OES

Calibration mode	variables		calibration		assumptions	analysis of unknowns: normalization needed
	independent	measured	cal. function ¹	cal. parameter for the linear term		
'normal' (mode 1)	$c_{E,M}$	$I_{E,M}$	Eqn. (1) ²	$\alpha_E = R_E q_M$	$q_M \approx \text{const}$	no
'ratio' (mode 2)	$c_{E,M}$	$\frac{I_{E,M}}{I_{P,M}}$	Eqn. (3) ²	$\beta_E = \frac{1}{c_{P,M}} \frac{R_E}{R_P}$	$c_{P,M} \approx \text{const},$ $c_{E,M} \gg (\text{BEC})_E$ $I_P = R_P c_{P,M} q_M^3$	no
'normalized' (mode 3)	$\frac{c_{E,M}}{c_{P,M}}$	$\frac{I_{E,M}}{I_{P,M}}$	Eqns. (4) ² , (22)	$\gamma_E = \frac{R_E}{R_P}$	$c_{E,M} \gg (\text{BEC})_E,$ $I_P = R_P c_{P,M} q_M^3$	yes (to calculate c_P)
'sputter rate- corrected'	$c_E q_M$	$I_{E,M}$	Eqns. (2) ² , (13)	R_E	q_M -s of calibration samples must be known or calculated	yes (to calculate q_M)

¹linear approximation (the measured variable as a linear function of the independent variable)²basic equation without the absolute term (background) and without corrections for line interferences³this relation for the reference line $\lambda(P)$ must hold accurately (linear intensity response, no line interferences, no matrix effects)

Table 3

Line interferences and their magnitudes (α_{EF}^{λ}) in the determination of tantalum and hafnium in nickel alloys¹

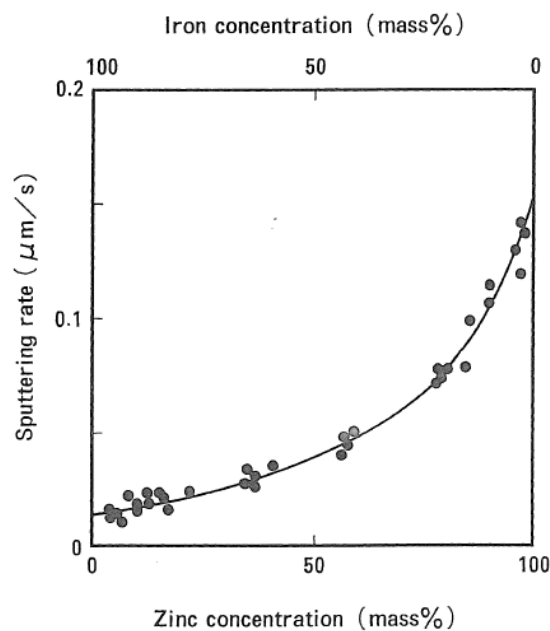
Instrument used: LECO GDS500A

Line		Interfering elements									
	λ / nm	Co	Cr	Fe	Mo	Nb	Ni	Ta	Ti	V	W
Hf II	282.023				0.070	0.027		0.009	0.45	0.053	0.015
Hf II	325.997	0.012		0.025	0.037	0.033		0.023	0.029	0.072	0.10
Hf I	368.224	0.005		0.031	0.006	0.016		0.003			0.062
Hf	376.27			0.022	0.017	0.038	0.021		0.15		0.008
Hf II	391.809	0.007	0.033	0.015	0.043	0.016	0.009	0.043	0.028		0.021
Hf I	462.086	0.005	0.016		0.071	0.018		0.007	0.014	0.043	0.009
Ta	214.16				0.053	0.17		x			0.080
Ta I	360.741	0.018	0.045	0.031	0.017		0.039	x			0.021
Ta I	362.662	0.012	0.002	0.013	0.048	0.071	0.016	x	0.029	0.010	0.012
Ta I	400.683	0.078		0.11	0.054	0.042		x	0.12	0.084	0.090
Ta I	404.087	0.060		0.042	0.095	0.12		x	0.020		0.048
Ta I	406.140	0.036		0.022	0.050	0.74		x		0.045	0.007
Ta I	414.789	0.018	0.011	0.015	0.031	0.095		x	0.031	0.31	0.036
Ta I	439.845		0.015		0.11	0.084	0.025	x	0.079		0.022
Ta I	441.574		0.004	0.089	0.018	0.068		x	0.087	0.35	0.026
Ta I	457.431	0.009	0.005		0.012	0.15	0.005	x	0.003	0.016	0.001

¹ the α_{EF}^{λ} values were calculated with weight units for the concentrations and the sputtering rates

Fig. 1a

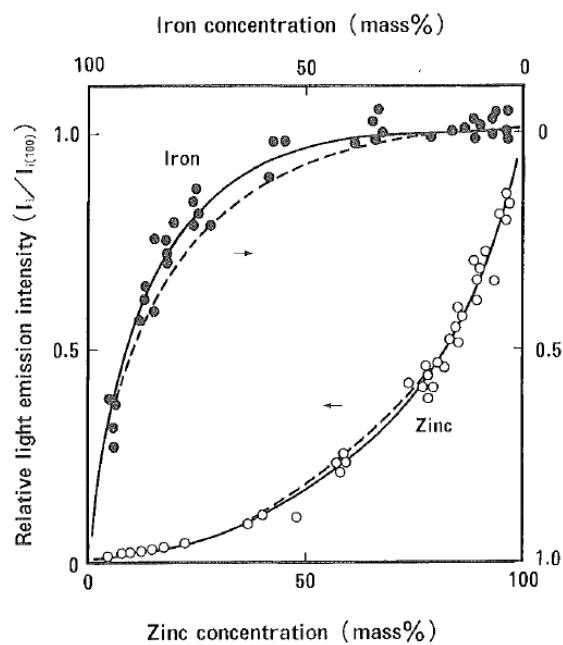
Sputtering rates of Zn-Fe binary alloys as function of the zinc concentration [21]



Reprinted from Ref. [2] with permission of Wiley. Copyright © 1997 by John Wiley & Sons Ltd.

Fig. 1b

Relative emission intensities in Zn-Fe binary alloys as function of the zinc concentration [21]



Reprinted from Ref. [2] with permission of Wiley. Copyright © 1997 by John Wiley & Sons Ltd.

Fig. 2

Calibration curve of the Mo I line at 418.832 nm for analysis of molybdenum in various nickel alloys Spectrometer LECO GDS500A, dc discharge in argon, effective spectral width of this channel was 0.07 nm. The turquoise points represent the raw data, the red points represent the corrected data (see the text)

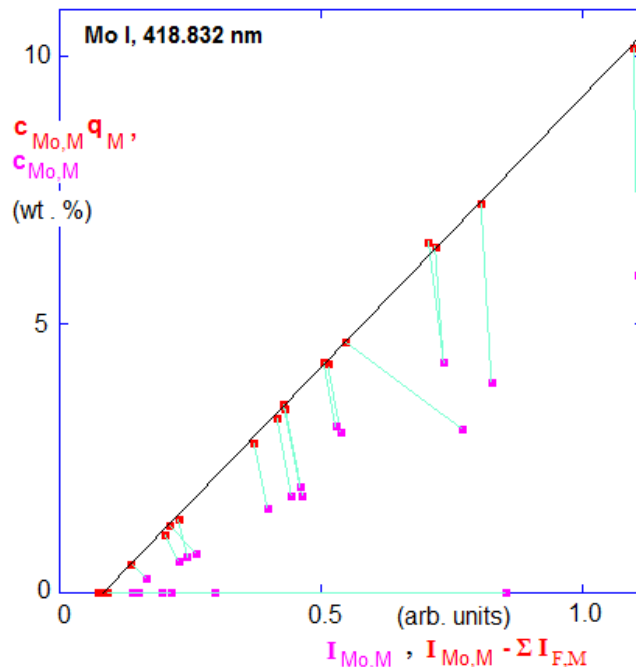


Fig. 3

Determination of the sputtering rate by measuring the erosion crater: pure magnesium in argon glow discharge, a 4mm-anode diameter, 700 V, 20 mA, $t = 265$ s: crater depth = $60.4 \mu\text{m}$, $Q_{Mg} = 4.98 \mu\text{g s}^{-1}$. Instrument used: 3D optical profiler Talysurf CCI Lite, Taylor-Hobson Ltd., UK

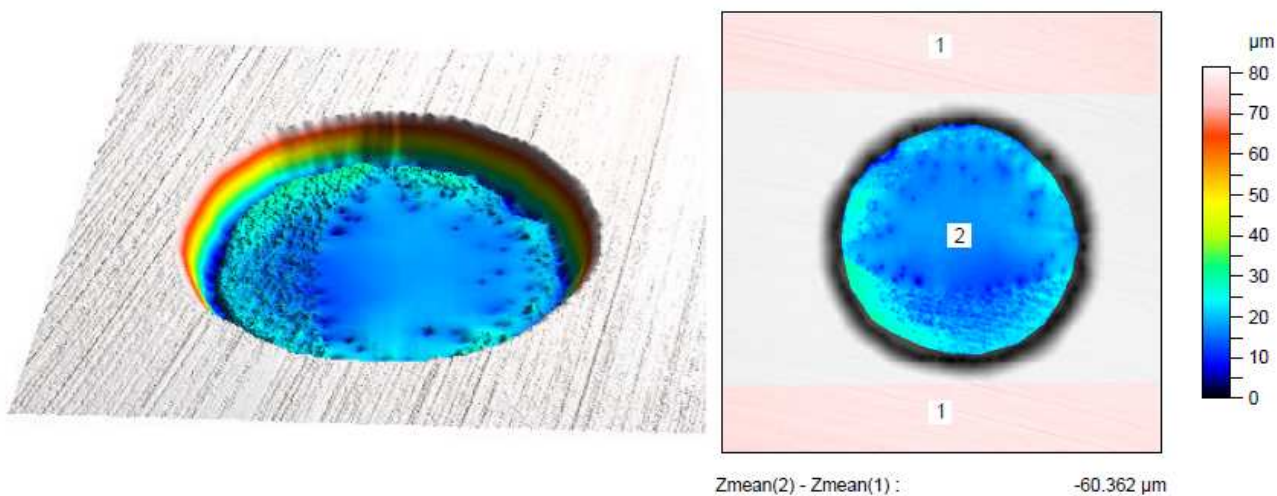


Fig. 4

Determination of a sputter factor from calibration functions: q_M was calculated for calibration sample IMZ-185 from the calibrations of the lines Co I, 240.725 nm (top) and Cr II, 283.563 nm (bottom)

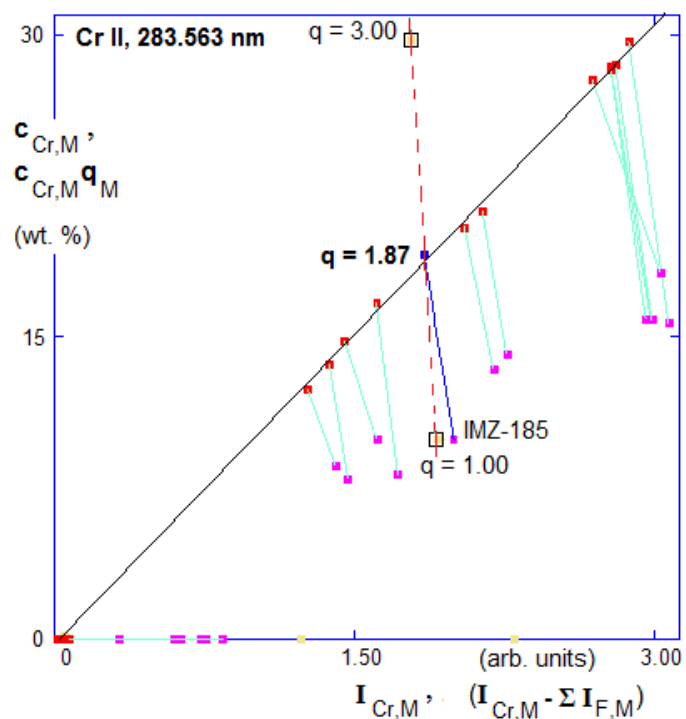
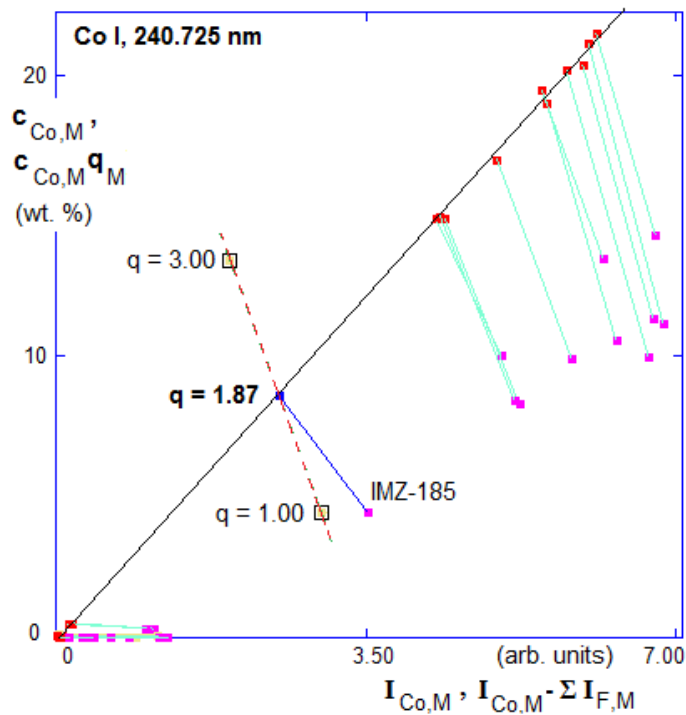


Fig. 5

Matrix effects in analysis of nickel in a set of nickel alloys: a line without matrix effects (Ni I, 301.200 nm, top) and a line with a matrix effect (Ni II, 216.910 nm, bottom)

